AMERICAN SOCIETY FOR MICROBIOLOGY | Journal of Virology®

PATHOGENESIS AND IMMUNITY

Porcine Circovirus Type 2 Induces ORF3-Independent Mitochondrial Apoptosis via PERK Activation and Elevation of Cytosolic Calcium

Yikai Zhang,[a] Renjie Sun,[a] Shichao Geng,[a] Ying Shan,[a] Xiaoliang Li,[a] Weihuan Fang[a]

[a]Institute of Preventive Veterinary Medicine and Zhejiang Provincial Key Laboratory of Preventive Veterinary Medicine, Zhejiang University, Hangzhou, China

ABSTRACT Our previous studies demonstrated that porcine circovirus type 2 (PCV2) triggers an unfolded protein response (UPR) in porcine kidney PK-15 cells by activating the protein kinase R-like endoplasmic reticulum kinase (PERK)/eukaryotic initiation factor 2α (eIF2α) pathway of endoplasmic reticulum (ER) stress, which in turn facilitates viral replication (Y. Zhou et al., Viruses 8:e56, 2016, https://doi.org/10.3390/v8020056; Y. Zhou et al., J Zhejiang Univ Sci B 18:316–323, 2017, https://doi.org/10.1631/jzus.B1600208). PCV2 is found to cause oxidative stress and upregulation of cytoplasmic Ca^{2+} levels. The virus is reported to employ its open reading frame 3 (ORF3) to induce apoptosis. We wondered whether and how PCV2-induced UPR would lead to apoptosis independent of ORF3. Using an ORF3-deficient PCV2 mutant (ΔORF3), apoptotic responses in infected PK-15 and porcine alveolar macrophage (PAM) cells were still apparent, although lower than in the parental PCV2 strain. We hypothesized that apoptosis induced by ΔORF3 might result from the UPR. We found that ΔORF3-induced apoptosis was significantly reduced when the infected cells were treated with the selective PERK blocker GSK2606414 (GSK) or the general ER stress attenuator 4-phenylbutyrate (4-PBA). Such treatments also ameliorated elevation of cytoplasmic Ca^{2+} and reactive oxygen species (ROS) levels in PK-15 and PAM cells, two predisposing factors for apoptosis via disruption of the ER-mitochondrion units. Treatment of ΔORF3-infected cells with GSK and 4-PBA also decreased the mitochondrial Ca^{2+} load and increased the mitochondrial membrane potential (MMP). With transient expression of the structural protein capsid (Cap) in combination with PERK silencing, we found that Cap induced MMP collapse and mitochondrial apoptosis could result from the UPR and elevation of Ca^{2+} and ROS levels, which were inhibitable by downregulation of PERK. We propose that PCV2-driven ER stress is Cap dependent and could lead to mitochondrial apoptotic responses independent of ORF3 via perturbation of intracellular Ca^{2+} homeostasis and accumulation of ROS.

IMPORTANCE PCV2 encodes protein ORF3, a putative protein with proapoptotic activity. Our early studies showed that PCV2 infection triggers ER stress via selective activation of the PERK pathway, a branch of the ER stress pathways, in permissive cells for enhanced replication and infection increased cytosolic Ca^{2+} and ROS levels. Here we clearly show that PCV2 infection or Cap expression induces ORF3-independent apoptosis via increased cytosolic and mitochondrial Ca^{2+} levels and cellular ROS levels as a result of activation of the PERK pathway.

KEYWORDS ORF3, porcine circovirus 2, UPR activation, mitochondrial apoptosis

Porcine circovirus (PCV) is a small, nonenveloped, circular single-stranded DNA virus belonging to the genus *Circovirus* of the *Circoviridae* family (1). PCV2 is associated with a variety of clinical disorders, such as enteritis, pneumonia, dermatitis, and nephropathy syndrome in pigs, collectively termed PCV-associated disease (PCVAD) (2).

Citation Zhang Y, Sun R, Geng S, Shan Y, Li X, Fang W. 2019. Porcine circovirus type 2 induces ORF3-independent mitochondrial apoptosis via PERK activation and elevation of cytosolic calcium. J Virol 93:e01784-18. https://doi.org/10.1128/JVI.01784-18.

Editor Jae U. Jung, University of Southern California

Address correspondence to Weihuan Fang, whfang@zju.edu.cn.

Received 8 October 2018
Accepted 29 December 2018
Accepted manuscript posted online 16 January 2019
Published 21 March 2019

PCV2 infection is immunosuppressive, as shown by lymphoid depletion in lymph nodes of infected pigs (3), and poses a severe threat to the pig industry worldwide. The virus has a circular single-stranded DNA genome of about 1.7 kb that contains three major open reading frames (ORFs): ORF1 codes for the replicase (Rep) protein involved in viral replication, ORF2 for the capsid (Cap) protein, and ORF3 for a putative protein with proapoptotic activity (4, 5). Recent reports suggested that ORF4, a newly identified putative PCV2 protein, played a role in suppressing caspase activity and regulated $CD4^+$ and $CD8^+$ T lymphocytes during PCV2 infection (6) but could induce caspase-independent apoptosis (7). Apoptotic cell death could be one of the mechanisms of lymphoid depletion during PCV2 infection, although the role of proapoptotic ORF3 in PCV2 pathogenesis remains controversial (5).

Endoplasmic reticulum (ER) stress is initially shaped to reestablish ER homeostasis through activation of the unfolded protein response (UPR) via integrated intracellular signaling (8). ER stress activates the stress sensors activating transcription factor 6 (ATF6) (9), inositol-requiring enzyme 1 (IRE1) (10), and protein kinase R-like ER kinase (PERK) (11), which represent three branches of the UPR. Some viruses, such as hepatitis C virus (HCV) (12), hepatitis B virus (HBV) (13), and varicella-zoster virus (14), could manage to establish persistent infections by interacting with the UPR. Our previous work revealed that PCV2 infection could induce ER stress and the UPR via activation of PERK/eukaryotic initiation factor 2α (eIF2α) signaling, with induction of downstream ATF4 and C/enhancer-binding protein (EBP)-homologous protein (CHOP) (15). When ER stress is too severe or prolonged, the prosurvival function of the UPR turns into toxic signals, including elevation of cytoplasmic Ca^{2+} or reactive oxygen species (ROS) levels, ultimately leading to mitochondrial apoptosis (16). Ca^{2+} is stored mainly in the ER and plays an essential role in cell life and death decisions (17). Ca^{2+} signaling interacts with other cellular signaling systems, such as redox signaling, in response to elevation of ROS levels (18, 19). A number of viruses, such as HCV (20, 21) and human immunodeficiency virus (HIV) (22), could disrupt intracellular Ca^{2+} homeostasis and redox balance, which would lead to mitochondrial dysfunction or cell death. ROS are produced predominantly from the mitochondrial respiratory chain (23). Redox-dependent regulation of components of intracellular Ca^{2+} homeostasis influences the direction and/or the efficiency of Ca^{2+} signaling (24, 25).

PCV2 infection has been demonstrated to induce oxidative stress in cultured cells, and treatment with the antioxidant *N*-acetyl-L-cysteine (NAC) reduced levels of ROS generation and PCV2 replication in porcine kidney PK-15 cells (26). Recent studies in our laboratory revealed that PCV2 infection caused an autophagic response through Ca^{2+}-dependent activation of the calcium/calmodulin-dependent protein kinase kinase β (CaMKKβ)-5′-AMP-activated protein kinase (AMPK)-mechanistic target of rapamycin (mTOR) pathway (27) and the virus utilized its Cap protein to induce the UPR, with subsequent apoptosis, shown as significant reduction of antiapoptotic B-cell lymphoma 2 (Bcl-2) expression and increased caspase-3 cleavage (28). However, it remains unknown whether Ca^{2+} and ROS play roles in mediating the cross talk of UPR and apoptosis and whether Cap contributes to mitochondrion-related apoptosis.

Here we show that ER stress and the UPR are induced by infection of PK-15 and porcine alveolar macrophage (PAM) cells with different strains of PCV2. We found that ORF3-deficient PCV2 (ΔORF3) infection could still induce apoptosis, concurrent with increased levels of cellular ROS and Ca^{2+}. Treatment of ΔORF3-infected cells with the PERK phosphorylation inhibitor GSK2606414 (GSK) or with the ER stress inhibitor 4-phenylbutyrate (4-PBA) could block elevation of intracellular ROS and cytoplasmic Ca^{2+} levels, rescued the mitochondrial membrane potential (MMP), and alleviated apoptosis. PCV2 Cap expression induced elevation of cytoplasmic Ca^{2+} and cellular ROS levels as well as loss of MMP and apoptotic responses, which could be inhibited by downregulation of PERK. We concluded that PCV2 Cap could induce an apoptotic response independent of ORF3 via increased cytoplasmic Ca^{2+} and cellular ROS levels as a result of ER stress in the infected cells. Our results provide new insights into the mechanisms of PCV2-infected cell death through cross talk between ER stress and apoptosis.

RESULTS

Different PCV2 strains induced ER stress, UPR, and apoptosis. To determine whether different strains of PCV2b and PCV2d could induce the UPR and apoptosis, PK-15 cells were infected with the same multiplicity of infection (MOI) (MOI of 1). Flow cytometry and the terminal deoxynucleotidyltransferase-mediated dUTP-biotin nick end labeling (TUNEL) assay were used to determine levels of apoptosis. Western blotting was employed to detect the expression of targeted molecules in PCV2-infected cells. Figure 1 shows that expression of glucose-regulated protein 78 (GRP78), phosphorylated PERK (p-PERK), and phosphorylated eIF2α (p-eIF2α) was significantly increased in virus-infected cells, compared with uninfected controls (Fig. 1A to D), suggesting that virus infection induced ER stress and the UPR. The viruses also induced apoptotic responses of PK-15 cells, as shown by significant elevation of cleaved caspase-3 levels (Fig. 1A and B) and increased numbers of apoptotic cells (Fig. 1E to H). Of the four viral strains tested, the PCV2b strains (SY4 and YW) had more significant effects than the PCV2d strains (JH and LX). Previous work in our laboratory showed that PCV2 led to increased expression of p-PERK and p-eIF2α at a given MOI at 24 h postinfection (hpi), which increased with increasing time up to 48 hpi (15). We chose 48 hpi for subsequent experiments to determine the full activation of ER stress and the UPR pathway while examing the apoptotis responses.

ORF3-deficient PCV2 infection was still capable of inducing UPR and apoptosis in PK-15 and PAM cells. The ORF3 protein was found to cause apoptosis in PCV2-infected cells (4). We hypothesized that PCV2-induced apoptosis might occur independent of ORF3 as a result of persistent ER stress during viral infection. The PCV2b strain YW, a recent isolate that caused apparent UPR and apoptotic responses (Fig. 1), was used to construct an isogenic mutant through inactivation of the start codon of *orf3* (see Fig. S1 in the supplemental material). To detect whether the mutant virus ΔORF3 could induce PERK/eIF2α activation and apoptosis, PK-15 and PAM cells were infected with ΔORF3 or its parental strain. Figure 2 shows that the ORF3-deficient virus could still induce PERK/eIF2α activation, caspase 3 cleavage, and GRP78 expression (Fig. 2A to H) and apoptosis (Fig. 2I to L) in both PK-15 and PAM cells, although the responses were generally lower than those observed with the parental strain. These results suggested that PCV2 infection induced an apoptotic response independent of the ORF3 protein, probably via the UPR pathway.

PCV2b-ΔORF3 infection perturbed cellular Ca^{2+} homeostasis, reduced MMP, and increased cytosolic ROS levels. Early studies showed that PCV2 infection could lead to increased cytosolic calcium (27) and intracellular ROS (26) levels, as well as ER stress (15). We anticipated that such responses would involve changes of MMP and its Ca^{2+} load after virus infection for 48 h. We assessed relative levels of cytosolic and mitochondrial Ca^{2+}, intracellular ROS, and MMP in PK-15 cells infected with PCV2b-ΔORF3 (ΔORF3) or its parental strain (wild type [WT]). We found that infection with the ΔORF3 mutant or its parental strain could raise both cytosolic and mitochondrial Ca^{2+} levels significantly, compared to the uninfected controls, while the parental virus showed more pronounced effects (Fig. 3A to D). Such increases were time dependent with an extended period of viral infection from 24 to 48 h. Confocal microscopic imaging also confirmed an increased Ca^{2+} load in the mitochondria of the virus-infected cells (Fig. 3E). Infection with either ΔORF3 or its parental strain also resulted in more pronounced reduction of MMP with a longer period of infection, compared with mock-infected cells (Fig. 4A and B). Flow cytometric analysis revealed that cells infected with both viruses had higher levels of cytosolic ROS than the uninfected cells over the entire infection period up to 48 h, although the impact was more apparent with the parental virus infection (Fig. 4C and D). All of these results suggested that infection with either ΔORF3 or its parental PCV2 strain could induce ER stress and elevation of cytosolic Ca^{2+} levels that would be inevitably linked with mitochondrial Ca^{2+} overload, reduced MMP, and increased ROS generation.

Chemical inhibition of ΔORF3-induced ER stress and UPR remitted mitochondrial apoptosis. To examine whether the ORF3-deficient PCV2 induced mitochondrial

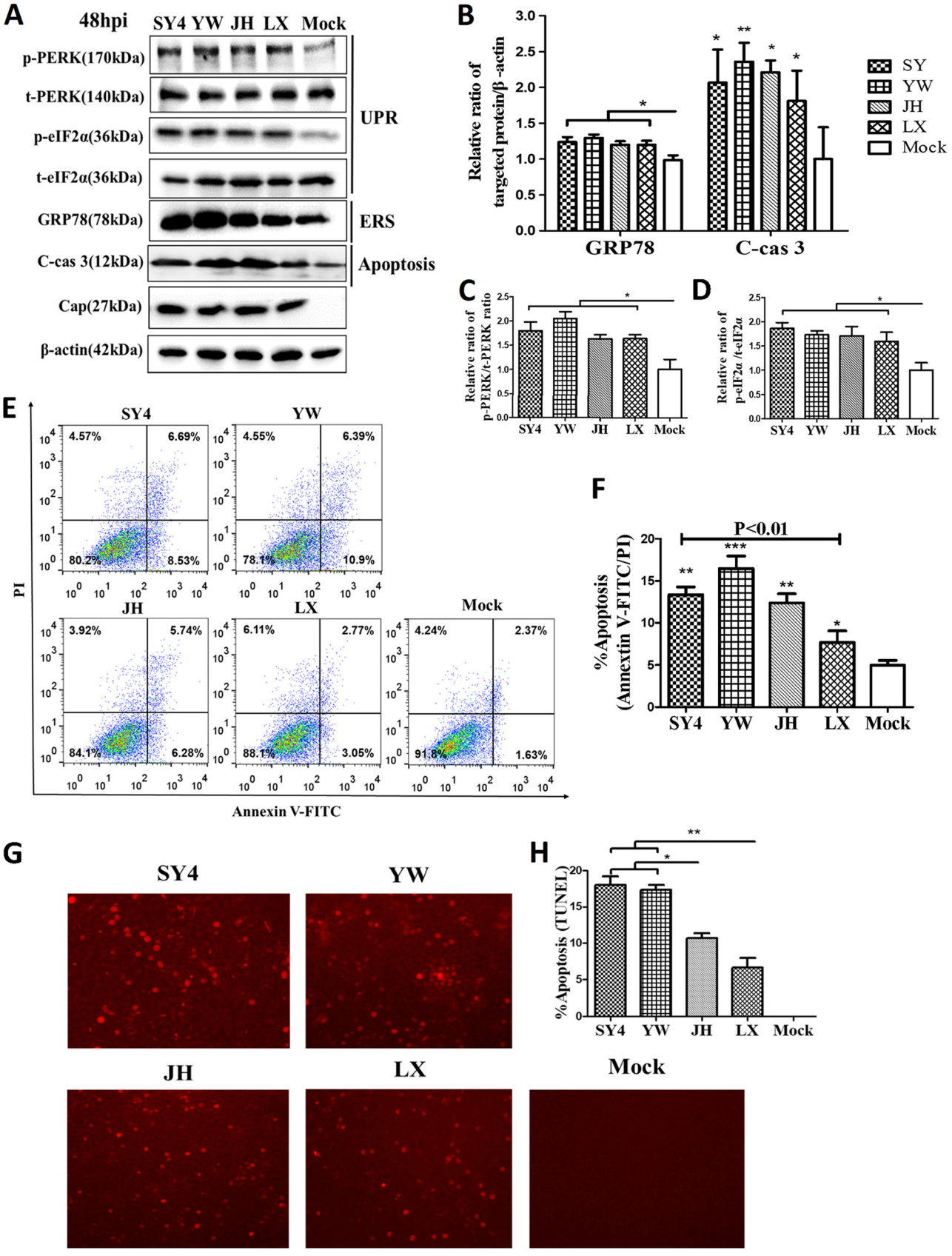

FIG 1 Different genotypes or strains of PCV2 induced different levels of ER stress, UPR, and apoptosis. PK-15 cells were infected with PCV2 for 48 h (MOI of 1). Strains SY4 and YW belong to PCV2b and the other two to PCV2d. Mock-infected cells were used as a sample loading control. (A) Cell extracts

(Continued on next page)

apoptosis via ER stress and UPR activation, GSK was used to block the UPR induced by virus infection and a small-molecule chemical chaperone (4-PBA), to relieve ER stress. Figure 5 shows that infection by the ΔORF3 mutant for 48 h led to significant increases in p-PERK, p-eIF2α, and cleaved caspase-3 levels, compared with mock-infected PK-15 or PAM cells. 4-PBA has drastic inhibitory effects on virus replication (Fig. 5A to H). GSK could significantly downregulate the levels of p-PERK and p-eIF2α induced by viral infection. The chemical 4-PBA had similar effects, although the effects were more pronounced with p-eIF2α than with p-PERK. Both chemicals could alleviate ΔORF3-induced apoptotic responses in PK-15 and PAM cells, as shown by reduced cleavage of caspase-3 (Fig. 5A to H) and by annexin V-fluorescein isothiocyanate (FITC)/propidium iodide (PI) and TUNEL assays (Fig. 5I to L). These findings indicated that ΔORF3-induced apoptosis is more likely the result of UPR activation during viral infection.

To support the aforementioned findings of the linkage between the ER and mitochondria in the ΔORF3-induced apoptotic response, the MMP and cytosolic Ca^{2+} and ROS levels were analyzed in virus-infected PK-15 or PAM cells treated with GSK or 4-PBA. Inhibition of the UPR or ER stress by the two chemicals could ameliorate virus-induced elevation of ROS levels (Fig. 6A and B), similar to the effect of NAC, an antioxidant known to have free-radical-scavenging property. Such treatments also alleviated MMP reduction (Fig. 6C and D) and led to diminution of cytosolic (Fig. 6E and F) and mitochondrial (Fig. 6G to J) Ca^{2+} levels. The effects of UPR or ER stress inhibitors on Ca^{2+} levels were similar to those of 2-aminoethoxydiphenyl borate (2-APB), an inositol 1,4,5-trisphosphate receptor (IP3R) blocker of Ca^{2+} efflux from the ER. Therefore, we suggest that ΔORF3-induced apoptosis might occur via mitochondrial alterations of Ca^{2+} levels, MMP, and ROS levels as a result of ER stress and UPR activation. GSK and 4-PBA could help maintain mitochondrial homeostasis and rescue virus-induced apoptosis by inhibiting ER stress.

Down-regulation of PERK mitigated PCV2- or Cap-induced mitochondrial apoptosis involving cellular Ca^{2+} imbalance and ROS generation. We showed previously that PCV2 Cap induced ER stress through increased phosphorylation of PERK, with subsequent activation of the eIF2α-ATF4-CHOP axis. Cap expression significantly reduced antiapoptotic Bcl-2 expression and increased caspase-3 cleavage (28). To determine whether PCV2 Cap could induce apoptosis via the mitochondrial pathway, cytosolic Ca^{2+} and ROS levels were analyzed by flow cytometry at 48 h in PK-15 cells transfected with pCMV-Cap (Fig. 7A) or infected with ΔORF3. Cap expression increased cytosolic Ca^{2+} and ROS levels and reduced the MMP (Fig. 7B to D). Caspase activation is the hallmark of apoptosis. We found that activities of caspase-3 and -9 were significantly higher in ΔORF3-infected cells and cells transfected with pCMV-Cap than in control cells (Fig. 7E and F). By flow cytometric analysis, we found that Cap expression induced significant cell apoptosis (Fig. 7G). Clearly, Cap-induced mitochondrial apoptosis involved Ca^{2+}, ROS, and perturbed MMP.

The relationship between UPR activation and apoptosis promoted us to examine the critical role of PERK in apoptosis induced by ORF3-deficient PCV2 infection or Cap expression. We silenced PERK via lentivirus-mediated short hairpin RNA (shRNA) transfer to PK-15 cells, which were then transfected with pCMV-Cap or infected with ΔORF3. Western blotting showed that downregulation of total PERK (t-PERK) expression was significant (Fig. 7H). Figure 7I and J show that downregulation of PERK could counteract the elevation of Ca^{2+} and ROS levels induced not only by ΔORF3 but also by Cap expression. Loss of MMP, activation of caspase-3 and -9, and apoptosis rates in

FIG 1 Legend (Continued)
were fractionated by SDS-PAGE and analyzed by Western blotting for p-PERK, t-PERK, p-eIF2α, t-eIF2α, GRP78, cleaved caspase 3 (C-cas 3), and Cap. β-Actin was used as a protein loading control. The gels shown here are representative of three individual experiments. (B to D) Ratios of GRP78 and cleaved caspase 3 to β-actin (B), p-PERK to t-PERK (C), and p-eIF2α to t-eIF2α (D) are shown. (E) PK-15 cells were stained with annexin V-FITC and PI for flow cytometric analysis. Apoptotic cells were divided into two stages, i.e., early apoptosis (annexin V positive and PI negative) and late apoptosis (annexin V negative and PI positive). (F) Total apoptosis rates examined using flow cytometry were quantified and are shown in a histogram. (G) TUNEL-stained cells indicated apoptosis via red fluorescence. (H) TUNEL-positive cells were counted in a total of >200 cells over six randomly selected fields. Data in the bar charts in panels B to D, F, and H represent the mean ± SEM of three independent experiments. *, $P < 0.05$; **, $P < 0.01$.

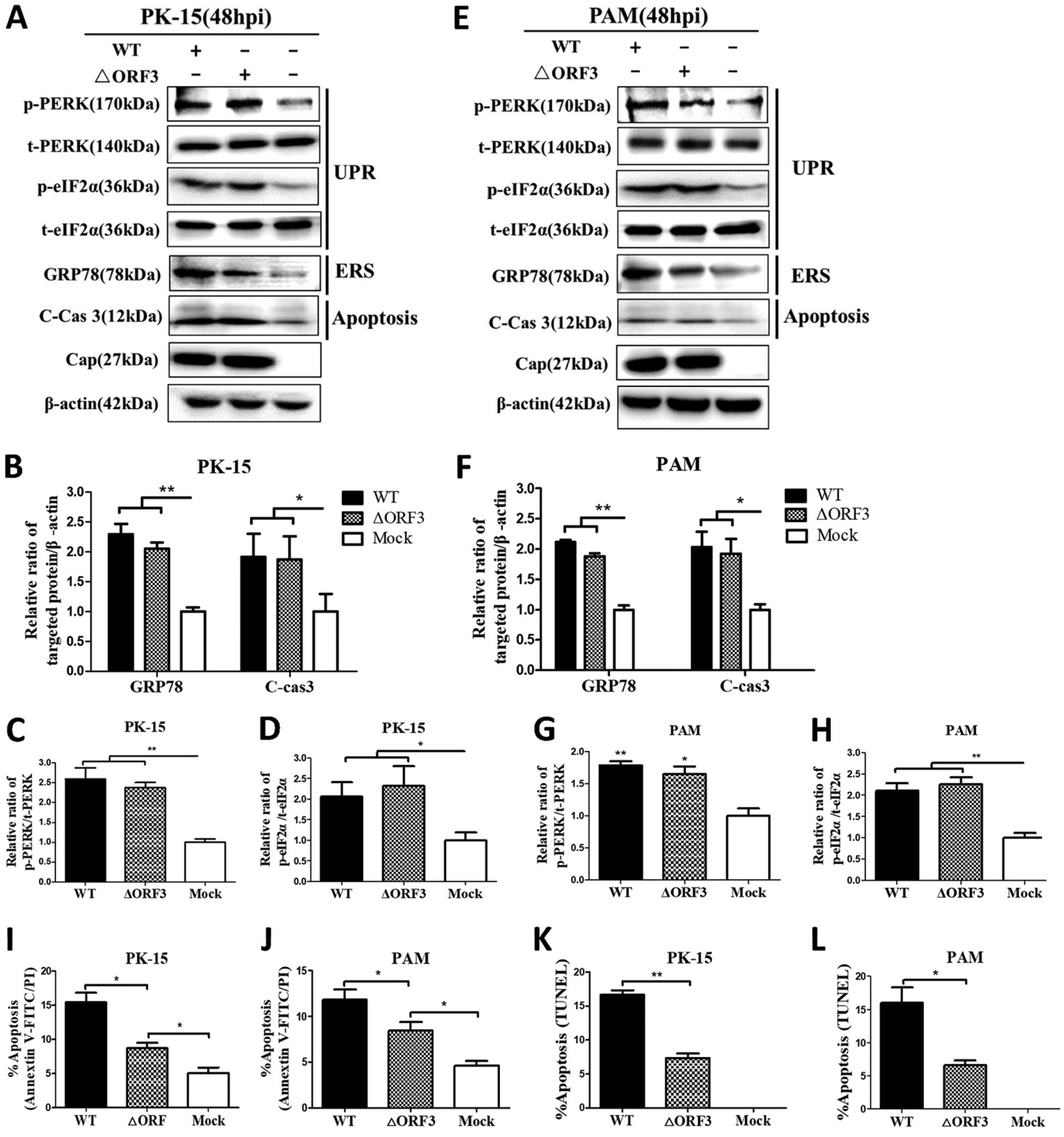

FIG 2 ORF3-deficient PCV2 mutant (ΔORF3) could activate the PERK/eIF2α pathway and induce ER stress and apoptosis in PK-15 and PAM cells. PK-15 and PAM cells were infected with PCV2b-YW (WT) or its mutant ΔORF3 for 48 h (MOI of 1). Mock-infected cells were used as a sample loading control (β-actin). (A) Target proteins of the PK-15 cell extracts were separated by SDS-PAGE and analyzed by Western blotting with antibodies to p-PERK, t-PERK, p-eIF2α, t-eIF2α, GRP78, cleaved caspase 3 (C-cas 3), and Cap. β-Actin was used as a protein loading control. The gels shown are representative of three individual experiments. (B to D) Ratios of GRP78 or cleaved caspase 3 to β-actin (B), p-PERK to t-PERK (C), and p-eIF2α to t-eIF2α (D) are shown. (E) Target proteins of the PAM cell extracts were separated by SDS-PAGE and analyzed by Western blotting as in panel A. (F to H) Ratios of GRP78 and cleaved caspase 3 to β-actin (F), p-PERK to t-PERK (G), and p-eIF2α to t-eIF2α (H) are shown. (I and J) Total apoptosis rates of PK-15 and PAM cells examined using flow cytometry were quantified and are shown in individual histograms. (K and L) TUNEL-positive PK-15 and PAM cells were counted in a total of >200 cells over six randomly selected fields. Data in the bar charts in panels B to D and F to L represent the mean ± SEM of three independent experiments. *, $P < 0.05$; **, $P < 0.01$.

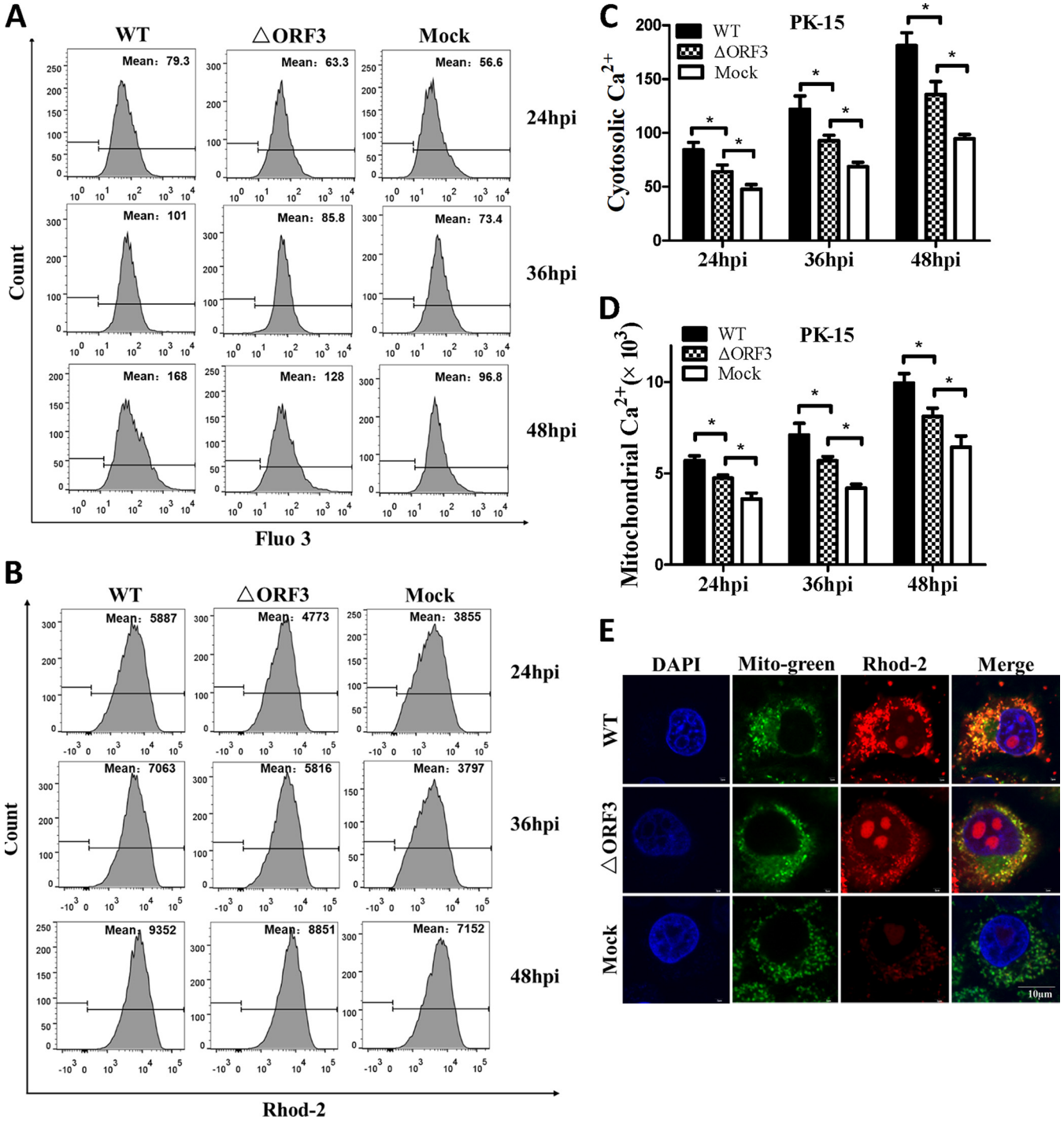

FIG 3 ORF3-deficient PCV2 mutant (ΔORF3) induced elevation of cytosolic and mitochondrial Ca^{2+} levels. PK-15 cells were infected with ΔORF3 or its parental strain PCV2b-YW (WT) at the same MOI (MOI of 1) for 24, 36, or 48 h. Mock-infected cells were used as a sample loading control. (A) Changes in cytosolic Ca^{2+} levels in PK-15 cells were measured by flow cytometry after incubation with 5 μM fluo-3/AM for 30 min at 37°C. (B) Changes in mitochondrial Ca^{2+} levels in PK-15 cells were measured by flow cytometry after incubation with 5 μM rhod-2 for 30 min at 37°C. (C and D) Changes in cytosolic and mitochondrial Ca^{2+} levels were evaluated according to the mean values of fluo-3 and rhod-2 fluorescence intensity. Data in the bar charts in panels C and D represent the mean ± SEM of three independent experiments. *, $P < 0.05$. (E) For confocal microscopy, serial treatments were followed with 5 μM rhod-2 for 30 min, 100 nM MitoBright Green dye for 15 min, and DAPI for 10 min in the dark after 48 hpi. Blue, nucleus; green, mitochondrial tracker; red: mitochondrial calcium tracker. Scale bar, 10 μm.

Cap-expressing or ΔORF3-infected cells were also inhibited by PERK knockdown (Fig. 7L to N). Thus, we propose that PCV2 might deploy its Cap to induce ER stress, which would ultimately lead to mitochondrial apoptosis by triggering the proapoptotic molecules Ca^{2+} and ROS.

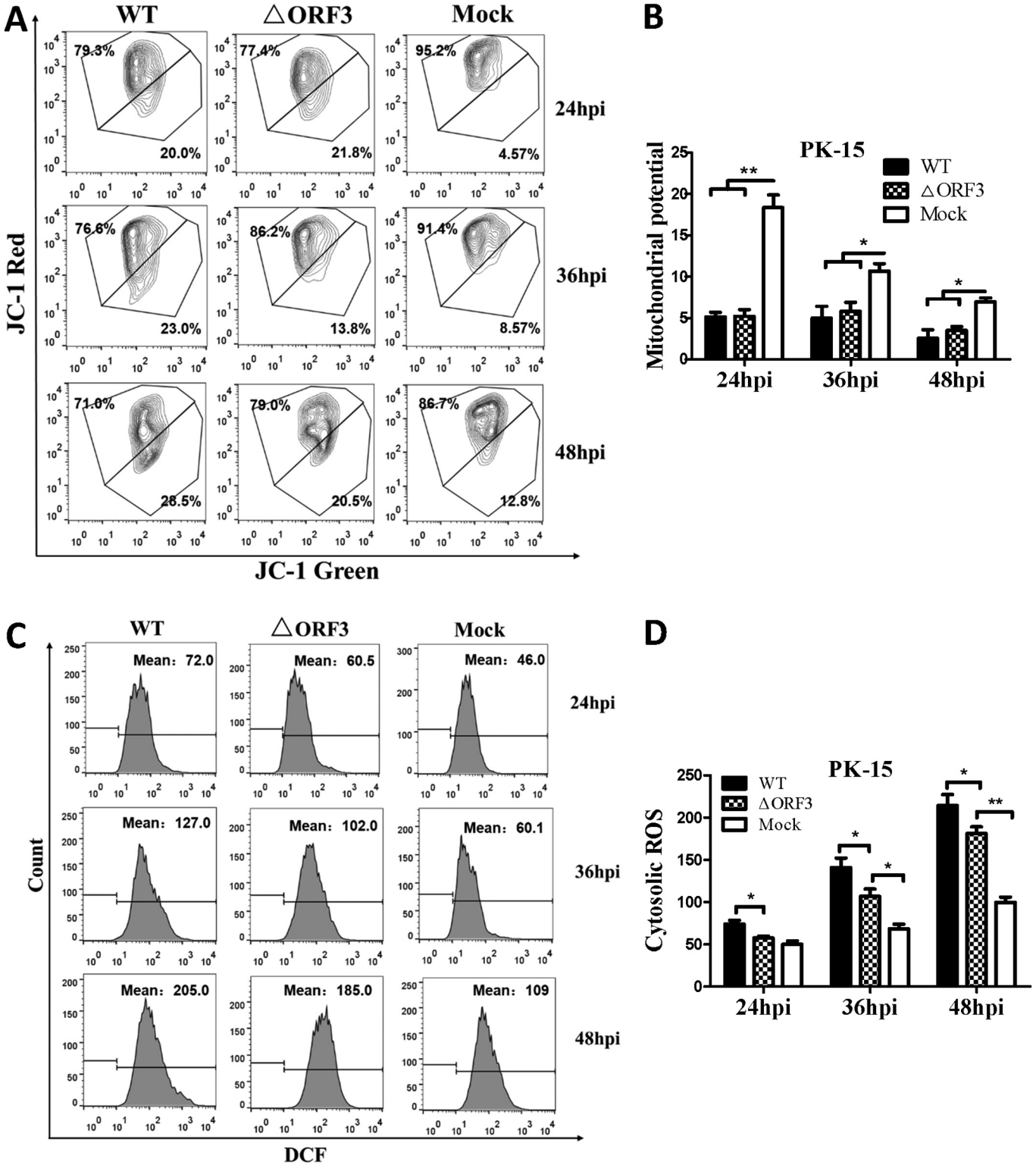

FIG 4 ORF3-deficient PCV2 mutant (ΔORF3) could induce cytosolic ROS accumulation and loss of MMP. PK-15 cells were infected with ΔORF3 or its parental strain PCV2b-YW (WT) at the same MOI (MOI of 1) for 24, 36, or 48 h. Mock-infected cells were used as a sample loading control. (A) Cells collected at 48 hpi were assessed for changes in MMP by flow cytometry after treatment with 5 μM JC-1 for 15 min at 37°C in the dark. (B) JC-1 fluorescence is depicted as the ratio between red and green fluorescence signals. (C) Cells collected at 48 hpi were assessed by flow cytometry for changes in cytosolic ROS levels after treatment with 10 μM DCFH-DA for 30 min at 37°C in the dark. (D) The changes in cytosolic ROS levels were evaluated according to the mean value of dichlorofluorescein (DCF) fluorescence intensity. Data in the bar charts in B and D represent the mean ± SEM of three independent experiments. *, $P < 0.05$; **, $P < 0.01$.

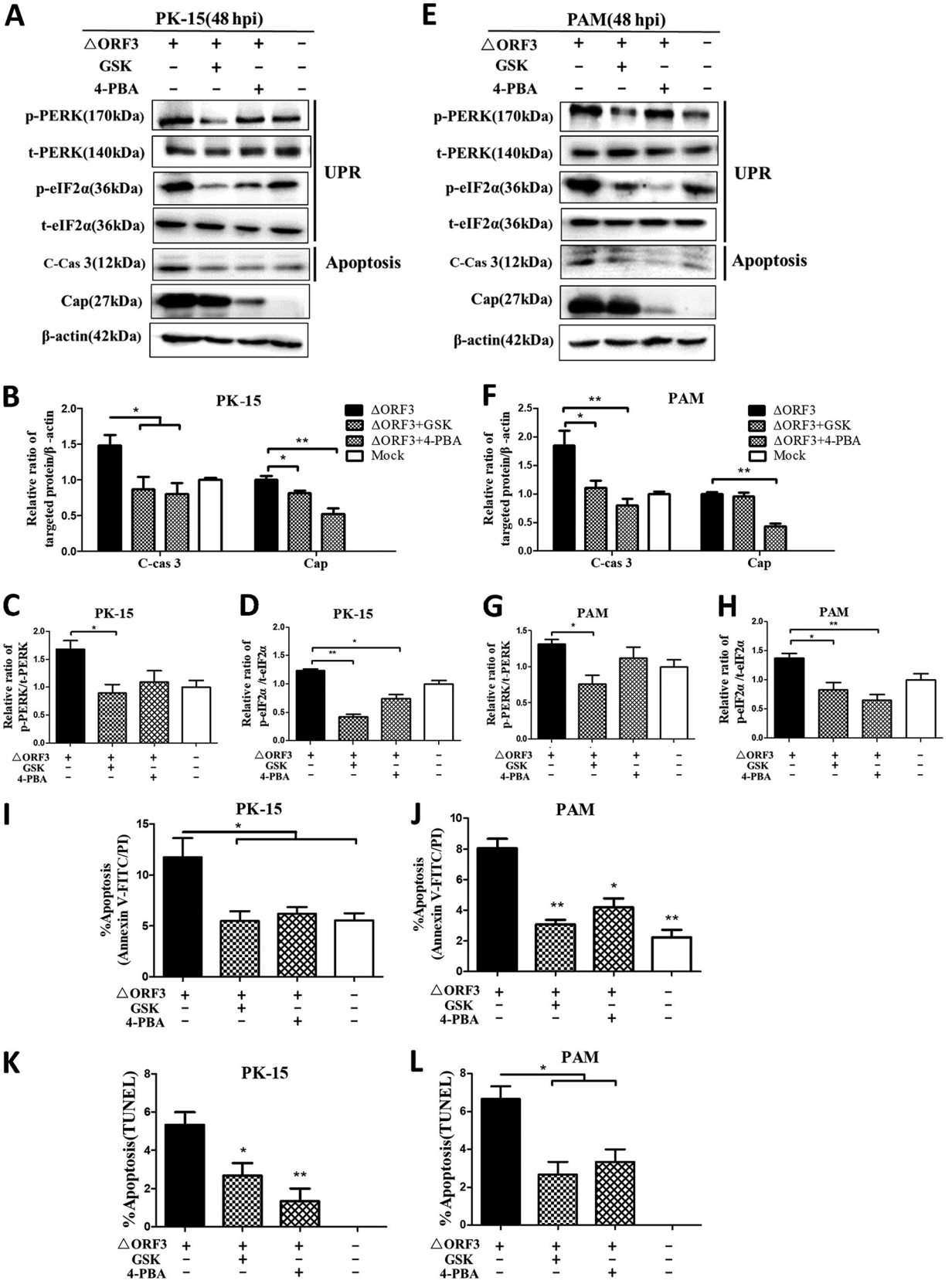

FIG 5 Apoptosis of PK-15 and PAM cells induced by ORF3-deficient PCV2 could be alleviated by blocking UPR or ER stress with chemical inhibitors. The cells were infected with ΔORF3 (MOI of 1), treated with 5 μM GSK or 2 mM 4-PBA at 2 hpi, and then incubated for an additional 46 h before measurement of target protein expression by Western blotting or apoptotic rate. (A) Target proteins of PK-15 cell extracts were separated by

(Continued on next page)

DISCUSSION

PCV2 is known to have significant reliance on the host cell machinery for its replication because of its small genome size, with limited coding proteins. Recent studies revealed that heat or oxidative stress could potentiate PCV2 replication (29, 30). We found that PCV2 infection could induce ER stress, which in turn facilitated viral replication in PK-15 cells (15). These findings, together with earlier observations of immune stimulation of viral replication (3), suggest that stress factors that perturb cellular responses are most likely in favor of PCV2 replication. Previous work in our laboratory showed that PCV2 infection initiated autophagy via activation of CaMKKβ by increased cytosolic Ca^{2+} levels (27) and that PCV2 utilizes its Cap protein to induce ER stress by PERK activation, which eventually leads to an apoptotic response (28). Because the ER is the major reservoir of Ca^{2+}, we postulate that PCV2-induced ER stress leads to a cellular Ca^{2+} imbalance that affects important cellular responses, including apoptosis. Here we clearly show that PCV2 infection or Cap expression induces ORF3-independent apoptosis via increased cytosolic and mitochondrial Ca^{2+} levels and cellular ROS levels as a result of activation of PERK, a branch of the ER stress pathways.

Ca^{2+} plays important roles in virus entry, viral gene expression, posttranslational processing of viral proteins, and virion maturation and release (31, 32). Ca^{2+} is an important activator of a number of proapoptotic proteases such as caspases and calpain (33, 34). HCV could induce oxidative stress-mediated Ca^{2+} imbalance (21). Meanwhile, increased cytosolic Ca^{2+} levels were found to activate CaMKKβ to initiate autophagy induced by PCV2, as shown in our recent study (27). Increased release of cytosolic Ca^{2+} from stressed ER by ORF3-deficient PCV2 would result in increased apoptosis as part of the cross talk between ER stress and apoptosis. However, the molecular basis linking PCV2- or Cap-induced ER stress with apoptosis remains unknown. Here we confirmed that ΔORF3 infection or Cap expression significantly induced cytosolic Ca^{2+} and ROS levels and caspase-3 and -9 activities, accompanied by a loss of MMP, which was preventable by downregulation of PERK either by inhibition of PERK phosphorylation with GSK or by short hairpin PERK (shPERK). Chemical treatment could have diverse effects other than the expected impact, particularly with 4-PBA, which could arrest the cell cycle and prevent the entry into S phase, favoring PCV2 replication (35, 36). To exclude the potential nonspecific effects of chemical treatment, we also used shRNA to specifically silence PERK expression. The results clearly indicate that Ca^{2+} signaling during PERK activation is engaged in apoptotic responses induced by PCV2 and its Cap.

Ca^{2+} signaling is known to interact with other cellular signaling systems, such as ROS (19). PCV2 infection caused a time-dependent increase in ROS levels that was found to facilitate viral replication inhibitable by treatment with the antioxidant NAC or selenium (37). We did observe time-dependent and parallel increases of cytosolic Ca^{2+} and ROS levels in PK-15 cells infected with ORF3-deficient PCV2 or its parental strain, suggesting the linkage of the two signaling systems in PCV2-infected cells. HBV X protein could target Bcl-2 to increase intracellular Ca^{2+} levels and viral DNA replication (38). Both Ca^{2+} and ROS contribute to apoptosis via a number of mechanisms, including mitochondrial dysfunction due to loss of MMP, altered interactions among proapoptotic and antiapoptotic Bcl-2 family proteins, and Ca^{2+}-dependent proteases (39–41). We found that apoptosis in ORF3-deficient PCV2-infected or Cap-expressing cells was significantly decreased when PERK phosphorylation was inhibited by GSK or t-PERK was downregulated by shRNA. Such effects were accompanied by reduced

FIG 5 Legend (Continued)
SDS-PAGE and analyzed by Western blotting for p-PERK, t-PERK, p-eIF2α, t-eIF2α, cleaved caspase 3 (C-cas 3), and Cap. β-Actin was used as a protein loading control. The gels shown are representative of three individual experiments. (B to D) Ratios of cleaved caspase 3 and Cap to β-actin (B), p-PERK to t-PERK (C), and p-eIF2α to t-eIF2α (D) are shown. (E) Target proteins of PAM cell extracts were separated by SDS-PAGE and analyzed by Western blotting for the same target proteins as in panel A. (F to H) Ratios of the target proteins as in panels B to D are shown. (I and J) Total apoptosis rates of PK-15 and PAM cells examined using flow cytometry were quantified and are shown in individual histograms. (K and L) TUNEL-positive cells were counted in a total of >200 cells over 6 randomly chosen fields. The data in the bar charts in panels B to D and F to L represent the mean ± SEM of three independent experiments. *, $P < 0.05$; **, $P < 0.01$.

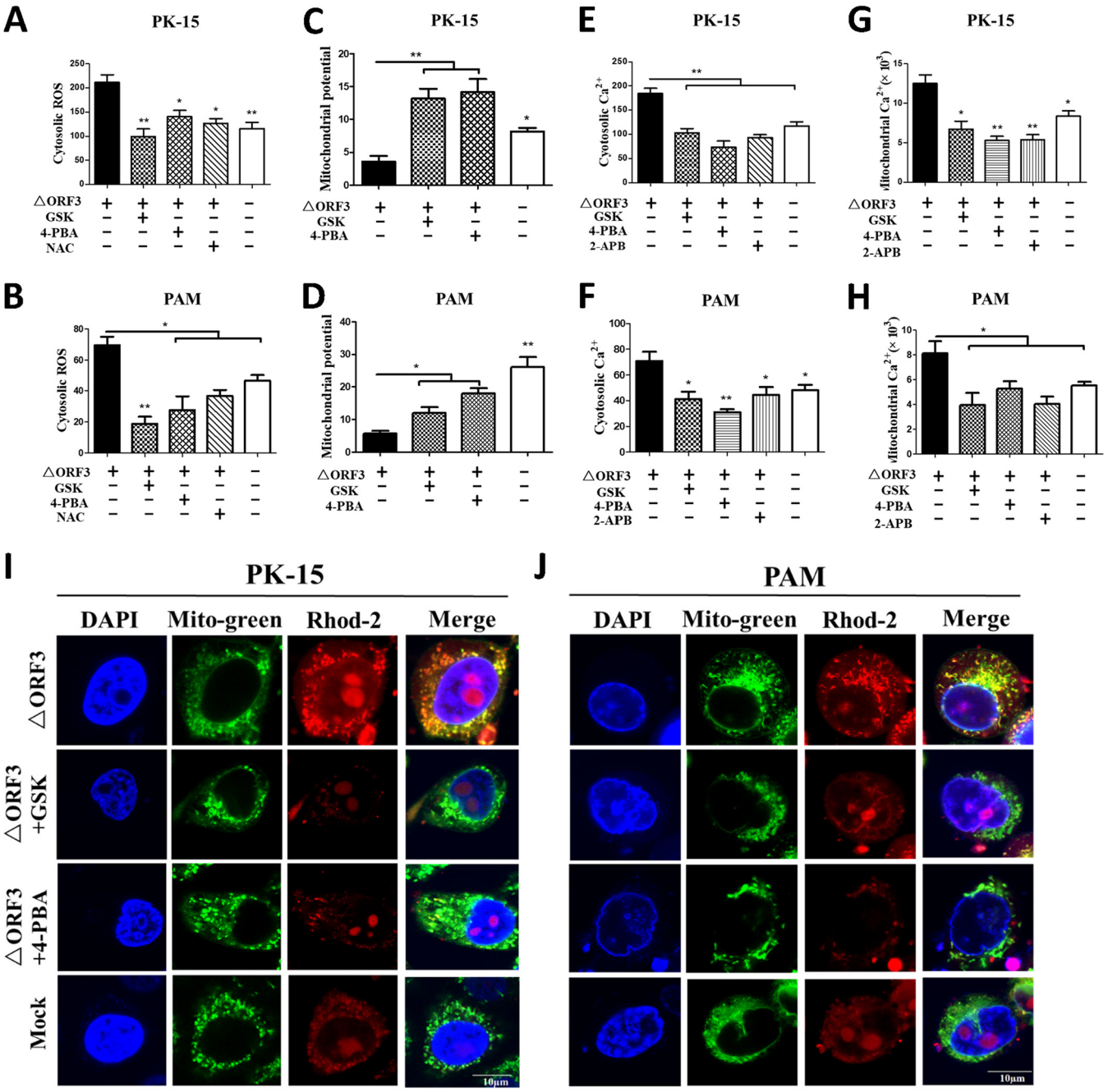

FIG 6 Blocking UPR or ER stress by chemical inhibitors decreased cellular ROS levels, increased MMP, and reduced cytosolic and mitochondrial Ca^{2+} levels in PK-15 and PAM cells infected with ORF3-deficient PCV2. PK-15 and PAM cells were incubated in 24-well plates. Cells were infected with ΔORF3 (MOI of 1), treated with 5 μM GSK or 2 mM 4-PBA at 2 hpi, and then incubated for an additional 46 h. The chemicals 2-APB (50 μM, as a Ca^{2+} channel IP3R inhibitor) and NAC (10 mM, as a ROS scavenger) were used as controls. (A and B) The changes in cytosolic ROS levels in PK-15 and PAM cells were evaluated according to the mean values of DCF fluorescence intensity. (C and D) JC-1 fluorescence is shown as the ratio between red and green fluorescence signals. (E to H) The changes in cytosolic and mitochondrial Ca^{2+} levels were evaluated according to the mean values of fluo-3 and rhod-2 fluorescence intensity. (I and J) By confocal microscopy, serial treatments were followed with 5 μM rhod-2 for 30 min, 100 nM MitoBright Green dye for 15 min, and DAPI for 10 min in the dark after 48 hpi. Blue, nucleus; green, mitochondrial tracker; red, mitochondrial calcium tracker. Scale bars, 10 μm. Data in the bar charts in panels A to H represent the mean ± SEM of three independent experiments. *, $P < 0.05$; **, $P < 0.01$.

levels of cytosolic and mitochondrial Ca^{2+} and cellular ROS, as well as increased MMP (Fig. 8). GSK is known to attenuate the UPR and ER-stress-mediated apoptosis in human ovarian cancer cells and cardiac muscle cells (42). Therefore, we tend to think that there is a link between the PCV2-induced UPR and mitochondrial apoptosis.

In summary, our data provide a novel mechanism of PCV2-induced apoptosis

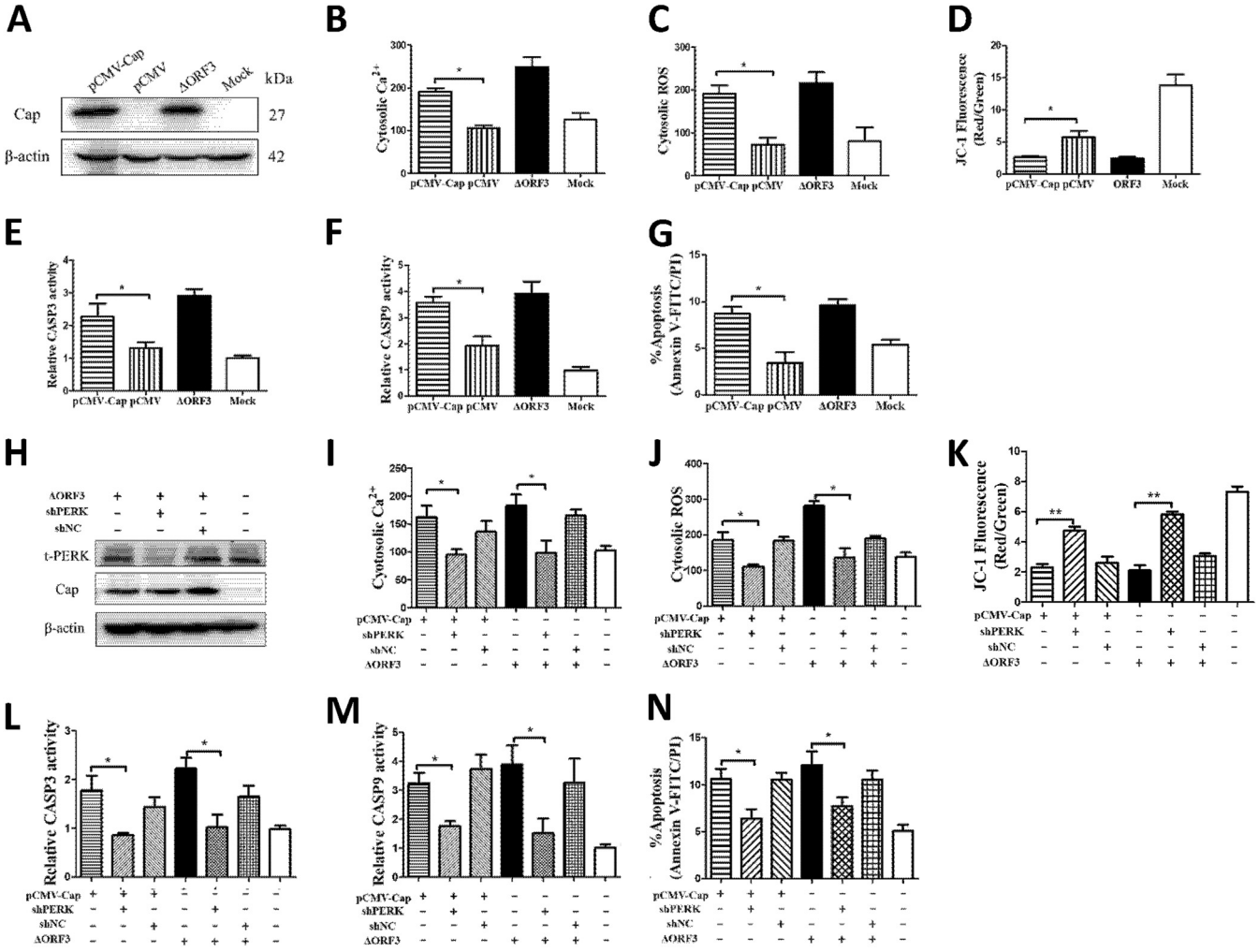

FIG 7 Silencing of PERK by lentivirus-mediated shRNA rescued mitochondrial apoptosis of PK-15 cells induced by ORF3-deficient PCV2 infection or Cap expression. PK-15 cells were infected with the lentivirus containing selective shPERK for 12 h and then were infected with ΔORF3 or transfected with pCMV-Cap (with the empty vector pCMV as a control) for 48 h to assess the relationship between Cap expression and mitochondrial apoptosis. (A and H) Cap expression and PERK silencing were detected by Western blotting. (B and I) The changes in cytosolic Ca^{2+} levels were evaluated according to the mean values of fluo-3 fluorescence intensity. (C and J) The changes in cytosolic ROS levels were evaluated according to the mean values of DCF fluorescence intensity. (D and K) JC-1 fluorescence is shown as the ratio between red and green fluorescence signals. (E, F, L, and M) The bar charts show fold changes of caspase-3 and -9 enzyme activities in cells. (G and N) Total apoptosis rates examined using flow cytometry were quantified and are shown as histograms. Data in the bar charts in panels B to G and I to N represent the mean ± SEM of three independent experiments. *, $P < 0.05$; **, $P < 0.01$.

through activation of ER stress and an UPR mediated by Ca^{2+} and ROS independent of the ORF3 protein, which was reported previously to have a direct contribution to apoptosis (4). Further work is under way to determine the molecular mechanisms of how Ca^{2+} and/or ROS facilitate PCV2 replication, an event within a vicious cycle leading to persistent or aggravated viral infection. The cross talk among ER stress, autophagy, and apoptosis during PCV2 infection also requires further investigation.

MATERIALS AND METHODS

Cells and viruses. Porcine kidney PK-15 cells and PAM cells free of PCV1 were used. The cells were cultured at 37°C with 5% CO_2 in Dulbecco's modified Eagle's medium (DMEM) containing 4% heat-inactivated fetal bovine serum with 1% L-glutamine, 1% nonessential amino acids, 100 U/ml penicillin G, and 100 μg/ml streptomycin.

The PCV2 strains SY4 (GenBank accession no. GU325754), YW (GenBank accession no. MG245866), JH (GenBank accession no. MG245867), and LX (GenBank accession no. MG870195) were originally isolated from the lungs of pigs with naturally occurring PCVAD in Zhejiang Province, China, and were propagated in PK-15 cells. The virus stocks contained $1 \times 10^{5.5}$, $1 \times 10^{5.25}$, $1 \times 10^{5.67}$, and $1 \times 10^{5.75}$ infectious virus particles per ml respectively. The SY4 and YW strains belong to PCV2b and the JH and LX strains to

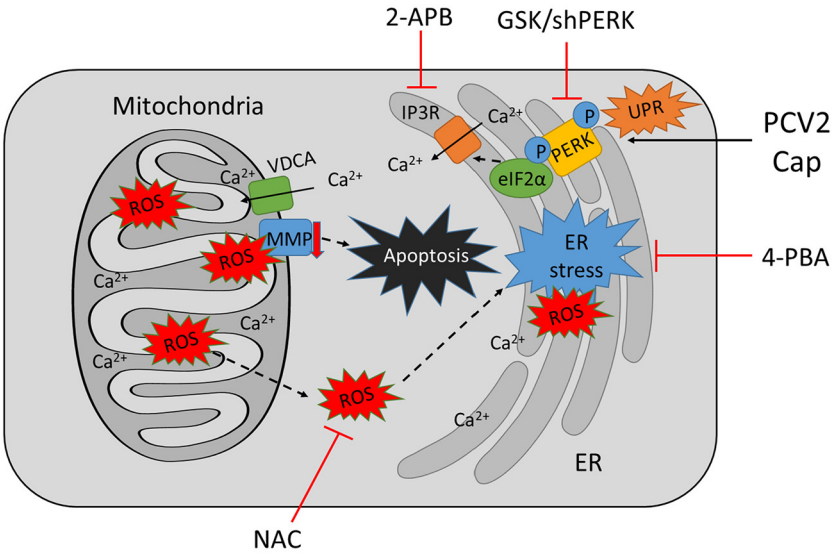

FIG 8 Proposed model of mitochondrial apoptosis induced by PCV2b-ΔORF3 infection or Cap expression via PERK activation and imbalance of cytosolic and mitochondrial calcium levels. PCV2b-ΔORF3 infection or Cap expression induces ER stress by PERK signaling, facilitates Ca^{2+} efflux from the ER, and increases mitochondrial Ca^{2+} levels, leading to mitochondrial dysfunction characterized as increased generation of ROS and loss of MMP, with eventual mitochondrial apoptosis. Treatment of PCV2b-ΔORF3-infected or Cap-expressing cells with the PERK phosphorylation inhibitor GSK (possibly with 4-PBA as an ER stress inhibitor) or silencing of PERK could suppress PCV2- or Cap-induced apoptosis by decreasing Ca^{2+} efflux and reducing ROS levels.

PCV2d. The genotype PCV2d is characterized by a mutation in the last codon of the *cap* gene, resulting in a 3-nt longer *orf2* (705 nt) (43).

The PCV2b strain YW, a recent isolate that causes an apparent UPR and apoptotic response (Fig. 1), was used to construct an isogenic mutant (ΔORF3). Primers muORF3-for (5′-AACCACTTCTTCACCGTGGT AACCATCCCACCA-3′) and muORF3-rev (5′-TGGTGGGATGGTTACCACGGTGAAGAAGTGGTT-3′) were designed to mutate the start codon of ORF3 from ATG to GTG, to nullify *orf3*. The mutant strain contained $1 \times 10^{5.25}$ infectious virus particles per ml (see Fig. S1 in the supplemental material).

Chemical inhibitors and antibodies. The chemicals 2-APB (as an IP3R inhibitor; Sigma-Aldrich), NAC (as a ROS scavenger; Beyotime), GSK (as a selective PERK inhibitor; Selleck), and PBA (Sigma-Aldrich) were used in appropriate experiments. The cell viability of PK-15 and PAM cells treated with the chemicals was assayed with cell counting kit 8 (Dojindo), following the manufacturer's instruction. Previous studies showed that treatment with these chemicals did not have significant effects on the viability of PK-15 and PAM cells (15, 27, 28).

Antibodies against β-actin, caspase-3A/B, total eIF2α (t-eIF2α), p-eIF2α, and p-PERK were purchased from Cell Signaling Technology. Antibodies against t-PERK and GRP78 were obtained from Proteintech. Mouse monoclonal anti-Cap antibody was produced in our laboratory. Goat anti-rabbit IgG or goat anti-mouse IgG secondary antibodies conjugated to horseradish peroxidase (HRP) were purchased from KPL.

Virus infection and chemical treatments. PK-15 cells at approximately 50% to 60% confluence were infected with different PCV2 strains (MOI of 1) for 48 h or were infected with an ORF3-deficient PCV2 mutant (ΔORF3) for different times, to analyze their ability to induce ER stress, the UPR, and apoptosis. To examine the effects of UPR or ER stress inhibitors on apoptosis, as well as on changes in levels of relevant molecules and MMP, PK-15 and/or PAM cells were first infected with ΔORF3 or its parental strain and then treated with different chemicals at 2 hpi. The cells were subjected to further incubation for specified times according to the experimental goals. All chemicals were added at the indicated concentrations (50 μM 2-APB, 10 mM NAC, 5 μM GSK, and 5 mM 4-PBA), with mock-infected cells as controls. All infected and/or treated cells were collected for the following assays.

Expression of PCV2 Cap- and lentivirus-mediated RNA interference. The cap gene *orf2* was cloned from the PCV2 YW strain and recombined into pCMV (Clontech) as pCMV-Cap. Delivery of the recombinant and control plasmids into PK-15 cells was performed by using Lipofectamine 2000 (Invitrogen), according to the manufacturer's instructions.

PK-15 cells were infected with the lentivirus containing specific shPERK (targeting sequence GCAG TCATCAGTTAGAATTTC) or short hairpin negative control (shNC) sequence (as a negative control) (GenePharma) for 12 h prior to coinfection with ΔORF3 (MOI of 1) or transfection with pCMV-Cap for an additional 48 h. All samples were harvested and subjected to Western blotting or labeled for flow cytometric analysis as described below.

Protein extraction and Western blotting. The cells in 24-well plates were washed three times with phosphate-buffered saline (PBS) (pH 7.2; Beyotime), treated with a cell lysis buffer (Beyotime) containing a cocktail of protease inhibitors (Roche), and scraped from the culture plate. The cell lysates were

centrifuged at 14,000 × *g* for 10 min at 4°C. Protein concentrations were determined using the Bradford assay. Equal amounts of protein samples were loaded and separated on 10% SDS–PAGE gels. The proteins in the gels were transferred to polyvinylidene fluoride (PVDF) membranes (Merck Millipore), which were then blocked with 5% nonfat milk powder in PBS containing 0.05% Tween 20 at 37°C for 1 h and incubated with different primary antibodies at 4°C overnight. Following this, the membranes were incubated for 1 h with appropriate secondary antibodies. Immunoreactive bands were visualized by using SuperSignal West Pico chemiluminescent substrate (Thermo Scientific), and images were captured with a Gel 3100 chemiluminescent imaging system (Sage Creation Science). The bands were quantified by densitometric analysis using NIH ImageJ software. Ratios of the target proteins to the reference proteins were used for relative quantitative purposes. Data are shown as the mean ± standard error of the mean (SEM) from three independent experiments.

Measurements of cytosolic Ca^{2+} and ROS levels, mitochondrial Ca^{2+} levels, and MMP. Cytosolic ROS and Ca^{2+} and mitochondrial Ca^{2+} levels in infected cells were probed using 10 μM 2′,7′-dichlorodihydrofluorescein diacetate (DCFH-DA) (Sigma-Aldrich), 5 μM fluo-3/acetoxy methyl (AM) (Dojindo), and 5 μM rhod-2/AM (Dojindo), respectively, in Hanks' balanced salt solution (HBSS) (Beyotime), for 30 min at 37°C in the dark. The cells were washed twice with HBSS, harvested after 0.25% trypsin treatment, collected by centrifugation (3 min at 500 × *g*), and resuspended in HBSS at a concentration of 10^6 cells/ml for flow cytometric analysis. All flow cytometric experiments were performed with a BD FACSCalibur flow cytometer (BD Biosciences) except for mitochondrial Ca^{2+} measurements in a BD FACS Aria flow cytometer (BD Biosciences). Data were analyzed using FlowJo software (version 10; TreeStar).

For MMP determinations, the infected cells at 48 h were probed with JC-1. JC-1 is a dye that exists in a monomeric form in nonpolarized mitochondria and fluoresces in the green spectrum (emission at 530 nm) when excited at 485 nm. The dye accumulates in the mitochondria based on the potential. This accumulation is accompanied by formation of dye aggregates, shifting fluorescence to the red spectrum (emission at 590 nm) when excited at 485 nm. Therefore, the red/green ratio indicates alterations in the mitochondrial potential between different cells or between treatments (44).

Confocal microscopic analysis of mitochondrial Ca^{2+} levels. For analysis of mitochondrial Ca^{2+} levels, PK-15 and PAM cells were cultured in petri dishes (10 mm in diameter; Xinyou) and infected with PCV2 at a MOI of 1. After incubation for 48 h, cells were loaded first with 5 μM rhod-2/AM for 30 min at 37°C and then with 100 nM MitoBright Green (a fluorescent probe from Dojindo for selective staining of mitochondria in living cells) for 15 min at 37°C. Finally, the double-labeled cells were treated with the nuclear dye 4′,6′-diamidino-2-phenylindole dihydrochloride (DAPI) (Beyotime). Cell images were captured by confocal microscopy (IX81-FV1000; Olympus).

Measurement of apoptosis. Apoptosis was detected using an annexin V-FITC apoptosis detection kit (Vazyme) and a TUNEL BrightRed apoptosis detection kit (Vazyme), following the manufacturer's instructions. After viral infection for 48 h, cells were trypsinized, washed twice in HBSS, resuspended in 1× binding buffer, and stained with annexin V-FITC and PI for 10 min at room temperature in the dark. At least 1 × 10^4 cells were evaluated using side and forward scattering to identify viable cell populations.

For the TUNEL assay, PK-15 cells were infected with PCV2 for 48 h in the absence or presence of 2-APB, NAC, GSK, or 4-PBA. Cells were fixed with 4% paraformaldehyde solution in PBS for 30 min at −20°C and then permeabilized with 0.1% Triton X-100 in 0.1% sodium citrate solution for 2 min on ice. The remaining steps were conducted following the manufacturer's instruction. The images (magnification of ×100) were captured by a computerized fluorescence microscope (IX71; Olympus).

To monitor cellular apoptosis as a function of caspase-3 and -9 activation, the caspase-3/9 activity assay kit (Beyotime) was used. The kit contains a lysis buffer with *N*-acetyl-Asp-Glu-Val-Asp-*p*-nitroanilide and *N*-acetyl-Leu-Glu-His-Asp-*p*-nitroanilide, caspase-3- and caspase-9-specific substrates that are cleaved upon exposure to active caspases and become fluorescent (excitation, 485 nm; emission, 530 nm).

Statistical analysis. Data are expressed as the mean ± SEM of three independent experiments. The statistical analyses were performed using GraphPad Prism 5. Statistical comparisons were made using one-way analysis of variance (ANOVA) followed by a least significant difference *post hoc* test. All statistical analyses were performed using SPSS 24.0. Differences were considered significant with P values of <0.05 and highly significant with P values of <0.01.

SUPPLEMENTAL MATERIAL

Supplemental material for this article may be found at https://doi.org/10.1128/JVI.01784-18.

SUPPLEMENTAL FILE 1, PDF file, 0.5 MB.

ACKNOWLEDGMENT

This work is part of a project sponsored by the National Natural Science Foundation of China (grant 31272534).

REFERENCES

1. Tischer I, Gelderblom H, Vettermann W, Koch MA. 1982. A very small porcine virus with circular single-stranded DNA. Nature 295:64–72.
2. Opriessnig T, Meng XJ, Halbur PG. 2007. Porcine circovirus type 2-associated disease: update on current terminology, clinical manifestations, pathogenesis, diagnosis, and intervention strategies. J Vet Diagn Invest 19:591–615. https://doi.org/10.1177/104063870701900601.

3. Meng XJ. 2013. Porcine circovirus type 2 (PCV2): pathogenesis and interaction with the immune system. Annu Rev Anim Biosci 1:43–64. https://doi.org/10.1146/annurev-animal-031412-103720.
4. Liu J, Chen I, Du Q, Chua H, Kwang J. 2006. The ORF3 protein of porcine circovirus type 2 is involved in viral pathogenesis in vivo. J Virol 80:5065–5073. https://doi.org/10.1128/JVI.80.10.5065-5073.2006.
5. Liu J, Chen I, Kwang J. 2005. Characterization of a previously unidentified viral protein in porcine circovirus type 2-infected cells and its role in virus-induced apoptosis. J Virol 79:8262–8274. https://doi.org/10.1128/JVI.79.13.8262-8274.2005.
6. He J, Cao J, Zhou N, Jin Y, Wu J, Zhou J. 2013. Identification and functional analysis of the novel ORF4 protein encoded by porcine circovirus type 2. J Virol 87:1420–1429. https://doi.org/10.1128/JVI.01443-12.
7. Lin C, Gu J, Wang H, Zhou J, Li J, Wang S, Jin Y, Liu C, Liu J, Yang H, Jiang P, Zhou J. 2018. Caspase-dependent apoptosis induction via viral protein ORF4 of porcine circovirus 2 binding to mitochondrial adenine nucleotide translocase 3. J Virol 92:e00238-18. https://doi.org/10.1128/JVI.00238-18.
8. Hetz C. 2012. The unfolded protein response: controlling cell fate decisions under ER stress and beyond. Nat Rev Mol Cell Biol 13:89–102. https://doi.org/10.1038/nrm3270.
9. Shen J, Snapp EL, Lippincott-Schwartz J, Prywes R. 2005. Stable binding of ATF6 to BiP in the endoplasmic reticulum stress response. Mol Cell Biol 25:921–932. https://doi.org/10.1128/MCB.25.3.921-932.2005.
10. Chen Y, Brandizzi F. 2013. IRE1: ER stress sensor and cell fate executor. Trends Cell Biol 23:547–555. https://doi.org/10.1016/j.tcb.2013.06.005.
11. Yan W, Frank CL, Korth MJ, Sopher BL, Novoa I, Ron D, Katze MG. 2002. Control of PERK eIF2α kinase activity by the endoplasmic reticulum stress-induced molecular chaperone P58IPK. Proc Natl Acad Sci U S A 99:15920–15925. https://doi.org/10.1073/pnas.252341799.
12. Wang J, Kang R, Huang H, Xi X, Wang B, Wang J, Zhao Z. 2014. Hepatitis C virus core protein activates autophagy through EIF2AK3 and ATF6 UPR pathway-mediated MAP1LC3B and ATG12 expression. Autophagy 10:766–784. https://doi.org/10.4161/auto.27954.
13. Lazar C, Uta M, Branza-Nichita N. 2014. Modulation of the unfolded protein response by the human hepatitis B virus. Front Microbiol 5:433–441. https://doi.org/10.3389/fmicb.2014.00433.
14. Carpenter JE, Grose C. 2014. Varicella-zoster virus glycoprotein expression differentially induces the unfolded protein response in infected cells. Front Microbiol 5:322. https://doi.org/10.3389/fmicb.2014.00322.
15. Zhou Y, Qi B, Gu Y, Xu F, Du H, Li X, Fang W. 2016. Porcine circovirus 2 deploys PERK pathway and GRP78 for its enhanced replication in PK-15 cells. Viruses 8:e56. https://doi.org/10.3390/v8020056.
16. Verfaillie T, Garg AD, Agostinis P. 2013. Targeting ER stress induced apoptosis and inflammation in cancer. Cancer Lett 332:249–264. https://doi.org/10.1016/j.canlet.2010.07.016.
17. Carreras-Sureda A, Pihán P, Hetz C. 2018. Calcium signaling at the endoplasmic reticulum: fine-tuning stress responses. Cell Calcium 70:24–31. https://doi.org/10.1016/j.ceca.2017.08.004.
18. Booth DM, Mukherjee R, Sutton R, Criddle DN. 2011. Calcium and reactive oxygen species in acute pancreatitis: friend or foe? Antioxid Redox Signal 15:2683–2698. https://doi.org/10.1089/ars.2011.3983.
19. Görlach A, Bertram K, Hudecova S, Krizanova O. 2015. Calcium and ROS: a mutual interplay. Redox Biol 6:260–271. https://doi.org/10.1016/j.redox.2015.08.010.
20. Quarato G, Scrima R, Ripoli M, Agriesti F, Moradpour D, Capitanio N, Piccoli C. 2014. Protective role of amantadine in mitochondrial dysfunction and oxidative stress mediated by hepatitis C virus protein expression. Biochem Pharmacol 89:545–556. https://doi.org/10.1016/j.bcp.2014.03.018.
21. Dionisio N, Garcia-Mediavilla MV, Sanchez-Campos S, Majano PL, Benedicto I, Rosado JA, Salido GM, Gonzalez-Gallego J. 2009. Hepatitis C virus NS5A and core proteins induce oxidative stress-mediated calcium signalling alterations in hepatocytes. J Hepatol 50:872–882. https://doi.org/10.1016/j.jhep.2008.12.026.
22. Agrawal L, Louboutin J-P, Marusich E, Reyes BAS, Van Bockstaele EJ, Strayer DS. 2010. Dopaminergic neurotoxicity of HIV-1 gpl20i reactive oxygen species as signaling intermediates. Brain Res 1306:116–130. https://doi.org/10.1016/j.brainres.2009.09.113.
23. Brookes PS, Yoon Y, Robotham JL, Anders MW, Sheu SS. 2004. Calcium, ATP, and ROS: a mitochondrial love-hate triangle. Am J Physiol Cell Physiol 287:C817–C833.
24. Gordeeva AV, Zvyagilskaya RA, Labas YA. 2003. Cross-talk between reactive oxygen species and calcium in living cells. Biochemistry (Mosc) 68:1077–1080.
25. Contreras L, Drago I, Zampese E, Pozzan T. 2010. Mitochondria: the calcium connection. Biochim Biophys Acta 1797:607–618. https://doi.org/10.1016/j.bbabio.2010.05.005.
26. Chen X, Ren F, Hesketh J, Shi X, Li J, Gan F, Huang K. 2012. Reactive oxygen species regulate the replication of porcine circovirus type 2 via NF-κB pathway. Virology 426:66–72. https://doi.org/10.1016/j.virol.2012.01.023.
27. Gu Y, Qi B, Zhou Y, Jiang X, Zhang X, Li X, Fang W. 2016. Porcine circovirus type 2 activates CaMMKβ to initiate autophagy in PK-15 cells by increasing cytosolic calcium. Viruses 8:135. https://doi.org/10.3390/v8050135.
28. Zhou Y, Gu Y, Qi B, Zhang Y, Li X, Fang W. 2017. Porcine circovirus type 2 capsid protein induces unfolded protein response with subsequent activation of apoptosis. J Zhejiang Univ Sci B 18:316–323. https://doi.org/10.1631/jzus.B1600208.
29. Liu J, Bai J, Zhang L, Jiang Z, Wang X, Li Y, Jiang P. 2013. Hsp70 positively regulates porcine circovirus type 2 replication in vitro. Virology 447:52–62. https://doi.org/10.1016/j.virol.2013.08.025.
30. Chen X, Ren F, Hesketh J, Shi X, Li J, Gan F, Hu Z, Huang K. 2013. Interaction of porcine circovirus type 2 replication with intracellular redox status in vitro. Redox Rep 18:186–192. https://doi.org/10.1179/1351000213Y.0000000058.
31. Zhou Y, Frey TK, Yang JJ. 2009. Viral calciomics: interplays between Ca^{2+} and virus. Cell Calcium 46:1–17. https://doi.org/10.1016/j.ceca.2009.05.005.
32. Clark KB, Eisenstein EM. 2013. Targeting host store-operated Ca^{2+} release to attenuate viral infections. Curr Top Med Chem 13:1916–1932.
33. González D, Espino J, Bejarano I, López JJ, Rodríguez AB, Pariente JA. 2010. Caspase-3 and -9 are activated in human myeloid HL-60 cells by calcium signal. Mol Cell Biochem 333:151–157. https://doi.org/10.1007/s11010-009-0215-1.
34. Sharma AK, Rohrer B. 2004. Calcium-induced calpain mediates apoptosis via caspase-3 in a mouse photoreceptor cell line. J Biol Chem 279:35564–35572. https://doi.org/10.1074/jbc.M401037200.
35. Xu D, Du Q, Han C, Wang Z, Zhang X, Wang T, Zhao X, Huang Y, Tong D. 2016. p53 signaling modulation of cell cycle arrest and viral replication in porcine circovirus type 2 infection cells. Vet Res 47:120–131. https://doi.org/10.1186/s13567-016-0403-4.
36. Li LZ, Deng HX, Lou WZ, Sun XY, Song MW, Tao J, Xiao BX, Guo JM. 2012. Growth inhibitory effect of 4-phenyl butyric acid on human gastric cancer cells is associated with cell cycle arrest. World J Gastroenterol 18:79–83. https://doi.org/10.3748/wjg.v18.i1.79.
37. Chen X, Ren F, Hesketh J, Shi X, Li J, Gan F, Huang K. 2012. Selenium blocks porcine circovirus type 2 replication promotion induced by oxidative stress by improving GPx1 expression. Free Radic Biol Med 53:395–405. https://doi.org/10.1016/j.freeradbiomed.2012.04.035.
38. Geng X, Huang C, Qin Y, McCombs JE, Yuan Q, Harry BL, Palmer AE, Xia NS, Xue D. 2012. Hepatitis B virus X protein targets Bcl-2 proteins to increase intracellular calcium, required for virus replication and cell death induction. Proc Natl Acad Sci U S A 109:18471–18476. https://doi.org/10.1073/pnas.1204668109.
39. Jeyaraju DV, Cisbani G, Pellegrini L. 2009. Calcium regulation of mitochondria motility and morphology. Biochim Biophys Acta 1787:1363–1373. https://doi.org/10.1016/j.bbabio.2008.12.005.
40. Webster KA. 2012. Mitochondrial membrane permeabilization and cell death during myocardial infarction: roles of calcium and reactive oxygen species. Future Cardiol 8:863–884. https://doi.org/10.2217/fca.12.58.
41. Nazıroğlu M, Yoldaş N, Uzgur EN, Kayan M. 2013. Role of contrast media on oxidative stress, Ca^{2+} signaling and apoptosis in kidney. J Membr Biol 246:91–100. https://doi.org/10.1007/s00232-012-9512-9.
42. Chen TC, Chien CC, Wu MS, Chen YC. 2016. Evodiamine from *Evodia rutaecarpa* induces apoptosis via activation of JNK and PERK in human ovarian cancer cells. Phytomedicine 23:68–78. https://doi.org/10.1016/j.phymed.2015.12.003.
43. Guo LJ, Lu YH, Wei YW, Huang LP, Liu CM. 2010. Porcine circovirus type 2 (PCV2): genetic variation and newly emerging genotypes in China. Virol J 7:273–284. https://doi.org/10.1186/1743-422X-7-273.
44. Perelman A, Wachtel C, Cohen M, Haupt S, Shapiro H, Tzur A. 2012. JC-1: alternative excitation wavelengths facilitate mitochondrial membrane potential cytometry. Cell Death Dis 3:e430. https://doi.org/10.1038/cddis.2012.171.